Colloidal Nanocrystals of Wurtzite $Zn_{1-x}Co_xO$ ($0 \leq x \leq 1$): Models of Spinodal Decomposition in an Oxide Diluted Magnetic Semiconductor

Michael A. White, Stefan T. Ochsenbein, and Daniel R. Gamelin*

Department of Chemistry, University of Washington, Seattle, Washington 98195-1700

Received August 22, 2008. Revised Manuscript Received October 7, 2008

Magnetic-ion-rich nanoscale inclusions formed by spinodal decomposition have been observed in many diluted magnetic semiconductors and have recently been implicated in the ferromagnetic ordering observed in some of these materials. In this study, colloidal nanocrystals of the ternary alloy wurtzite $Zn_{1-x}Co_xO$, with x ranging from 0.0 (w-ZnO) to 1.0 (w-CoO), have been synthesized as model systems for the proposed spinodal decomposition nanostrucures of ferromagnetic $Zn_{1-x}Co_xO$ thin films and powders. As free-standing nanocrystals, these phases do not show any signs of ferromagnetism or superparamagnetism at any value of x. Changes in the electronic absorption and magnetic circular dichroism (MCD) spectra with x are described that should allow optical identification of spinodal decomposition in other $Zn_{1-x}Co_xO$ samples. Optical and magneto-optical spectroscopic results are presented for the end member of this series (w-CoO), apparently for the first time, and show this binary oxide to be an indirect gap charge-transfer insulator with $E_g \approx 2.3$ eV.

I. Introduction

The magnetic properties of wide-gap diluted magnetic semiconductors (DMSs) are attracting broad interest in both fundamental and applied research areas.[1−4] High-temperature ferromagnetism is frequently reported for this class of materials, but its origins are still under debate. Recently, attention has been drawn to the possibility that the ferromagnetism of many DMSs might be associated with spinodal decomposition,[5−9] in which *isostructural* dopant-rich nanoscale domains embedded within a dopant-poor host matrix show cooperative magnetization and hysteresis. Spinodal decomposition is extremely difficult to study experimentally because detection generally requires ion-sensitive and spatially resolved techniques, preferably also with high magnetic sensitivity. In $Zn_{1-x}Cr_xTe$, for instance, the existence of such enrichments has been confirmed by a combination of transmission electron microscopy and energy dispersive X-ray spectroscopy, and parallel magnetization measurements have shown phenomenologically that the emergence of ferromagnetism is correlated with the spinodal decomposition.[7] Spinodal decomposition is also difficult to control experimentally. In $Zn_{1-x}Cr_xTe$, it was shown to be influenced by the position of the Fermi level, being facilitated by *n*-type doping and impeded by *p*-type doping.[7] Zinc blende CrTe is ferromagnetic,[10] explaining the ferromagnetism of dopant-enriched domains in $Zn_{1-x}Cr_xTe$.

Extension of these concepts to explain the high-T_C ferromagnetism of wurtzite $Zn_{1-x}Co_xO$ has been proposed.[5,11−13] In one study, the magneto-resistance and reduced paramagnetism of $Zn_{1-x}Co_xO$ films was proposed to arise from formation of Co^{2+}-enriched $Zn_{1-x}Co_xO$ domains with diameter $d < 10$ nm.[11] Superstatistical Co^{2+} clustering has been observed by EXAFS in $Zn_{1-x}Co_xO$ thin films prepared by pulsed laser deposition.[14] Neither the sizes nor the effective Co^{2+} cation mole fractions of these enrichments is known, and their relationship to ferromagnetism has not been demonstrated experimentally; that is, there has not yet been any experimental correlation between Co^{2+} enriched domains and ferromagnetism in $Zn_{1-x}Co_xO$. Although wurtzite cobalt oxide (w-CoO) is an antiferromagnet,[15−18] it may still be possible for Co^{2+}-enriched domains within $Zn_{1-x}Co_xO$ to

* Corresponding author. E-mail: gamelin@chem.washington.edu.

(1) Liu, C.; Yun, F.; Morkoc, H. *J. Mater. Sci.* **2005**, *16*, 555–597.
(2) Coey, J. M. D. *Curr. Opin. Solid State Mater. Sci.* **2006**, *10*, 83–92.
(3) Archer, P. I.; Gamelin, D. R. In *Magnetism in New Semiconducting and Insulating Oxides*; Hong, N. H., Ed.; Transworld Research Network: Kerala, India, 2007.
(4) Pan, F.; Song, C.; Liu, X. J.; Yang, Y. C.; Zeng, F. *Mater. Sci. Eng.* **2008**, *R62*, 1–35.
(5) Sato, K.; Katayama-Yoshida, H.; Dederichs, P. H. *Jpn. J. Appl. Phys.* **2005**, *44*, L948–L951.
(6) Fukushima, T.; Sato, K.; Katayama-Yoshida, H.; Dederichs, P. H. *Jpn. J. Appl. Phys.* **2006**, *45*, L416–L418.
(7) Kuroda, S.; Nishizawa, N.; Takita, K.; Mitome, M.; Bando, Y.; Osuch, K.; Dietl, T. *Nat. Mater.* **2007**, *6*, 440–446.
(8) Dietl, T. *J. Phys.: Condens. Matter* **2007**, *19*, 165204.
(9) Sato, K.; Fukushima, T.; Katayama-Yoshida, H. *Jpn. J. Appl. Phys* **2007**, *46*, L682–L684.
(10) Sreenivasan, M. G.; Teo, K. L.; Jalil, M. B. A.; Liew, T.; Chong, T. C.; Du, A. Y. *IEEE Trans. Magn.* **2006**, *42*, 2691–2693.
(11) Dietl, T.; Andrearczyk, T.; Lipinska, A.; Kiecana, M.; Tay, M.; Wu, Y. *Phys. Rev. B* **2007**, *76*, 155312.
(12) Sanyal, B.; Knut, R.; Grånäs, O.; Iuşan, D. M.; Karis, O.; Eriksson, O *J. Appl. Phys.* **2008**, *103*, 07D131.
(13) Nayak, S. K.; Ogura, M.; Hucht, A.; Buschmann, S.; Akai, H.; Entel, P. *Phys. Status Solidi A* **2008**, *205*, 1839–1846.
(14) Sun, Z.; Yan, W.; Zhang, G.; Oyanagi, H.; Wu, Z.; Liu, Q.; Wu, W.; Shi, T.; Pan, Z.; Xu, P.; Wei, S. *Phys. Rev. B* **2008**, *77*, 245208.
(15) Risbud, A. S.; Snedeker, L. P.; Elcombe, M. M.; Cheetham, A. K.; Seshadri, R. *Chem. Mater.* **2005**, *17*, 834–838.
(16) Seo, W. S.; Shim, J. H.; Oh, S. J.; Lee, E. K.; Hur, N. H.; Park, J. T. *J. Am. Chem. Soc.* **2005**, *127*, 6188–6189.
(17) An, K.; Lee, N.; Park, J.; Kim, S. C.; Hwang, Y.; Park, J. G.; Kim, J. Y.; Park, J. H.; Han, M. J.; Yu, J. J.; Hyeon, T. *J. Am. Chem. Soc.* **2006**, *128*, 9753–9760.

10.1021/cm802280g CCC: $40.75
Published on Web 11/06/2008

show cooperative magnetization (superparamagnetism or ferromagnetism) under certain conditions. For example, nanocrystals of antiferromagnetic materials can show substantial magnetic moments and hystereses due to uncompensated surface spins and appreciable anisotropy.[19] One illustrative case is NiO nanocrystals in the rock salt structure, which show ferromagnetic-like magnetization signatures for crystal diameters smaller than $d \sim 100$ nm.[20,21] Precisely this scenario has been proposed to explain the paradoxical observation of anisotropic ferromagnetism but lack of ferromagnetic signatures in electron transport in $Zn_{1-x}Co_xO$ films.[11]

This article describes the synthesis of structural and compositional analogues of the proposed enrichments of $Zn_{1-x}Co_xO$ that arise from spinodal decomposition, in the form of free-standing colloidal nanocrystals. These nanocrystals are the equivalent of excised spinodal enrichments and as such allow the physical properties of the proposed spinodal domains to be studied in concentrated form without contributions from other aspects of the matrix. The physical properties of colloidal $Zn_{1-x}Co_xO$ nanocrystals in the dilute doping limit ($x < \sim 0.02$) have been studied extensively in recent years,[22−29] but there has been little previous study of $Zn_{1-x}Co_xO$ nanocrystals (or films) in the heavily doped or intermediate alloy range that would be most relevant to spinodal decomposition (i.e., magnetic-ion rich rather than magnetic-ion pure). The physical properties of the end point in this series (w-CoO) have not been extensively studied because this is a meta-stable phase,[30] but prior experiments[15−18] and density functional calculations[31,32] have identified this phase as antiferromagnetic. Here, $Zn_{1-x}Co_xO$ nanocrystals across the series $0.0 \leq x \leq 1.0$ have been prepared by direct chemical synthesis. Structural and optical measurements have allowed the changes that occur as a function of x to be analyzed. Magnetization of w-CoO ($x = 1.0$) has been measured, and uncompensated surface spins have been detected; however, no evidence of any cooperative magnetization (i.e., superparamagnetism or ferromagnetism) could be detected. Furthermore, none of the other compositions ($x \neq 1.0$) showed any ferromagnetic-like properties. These results are inconsistent with scenarios in which spinodal decomposition alone leads to ferromagnetism in $Zn_{1-x}Co_xO$. If spinodal decomposition is a necessary condition for ferromagnetism in $Zn_{1-x}Co_xO$, then other factors such as additional charge carriers or structural defects must also be required to activate the ferromagnetism.

In the course of these studies, the optical properties of w-CoO were also investigated. The electronic absorption spectrum of w-CoO has apparently not been reported previously. From the electronic absorption and magnetic circular dichroism (MCD) spectroscopic data presented here, it is concluded that w-CoO has an indirect optical band gap energy of ~2.3 eV that is predominantly charge transfer in character, and it is shown that the Co^{2+} ions retain localized d-level electronic structures similar to those in dilute $Zn_{1-x}Co_xO$.

II. Experimental Section

Colloidal $Zn_{1-x}Co_xO$ nanocrystals were prepared following methods we have described in detail previously,[23] with the additional modification of a final surface passivation using oleylamine. Colloidal w-CoO nanocrystals were synthesized by adapting literature procedures that yield powders of this material[16,33] to now yield surfactant-capped nanocrystals that can be purified and handled as easily as colloids. Purification is important because of the risk of ferromagnetic impurity phases such as the metallic Co described in refs 15, 17, and 33. Briefly, colloidal w-CoO nanocrystals were prepared by decomposition of cobalt(II) acetylacetonate ($Co(acac)_2$) in oleylamine at 200 °C. Oleylamine (7.6 g, 28 mmol) was degassed at 135 °C for 1 h under vacuum. With an overpressure of nitrogen, $Co(acac)_2$ (50 mg, 0.2 mmol) was added to the oleylamine with vigorous stirring. When the purple powder had fully dissolved (~2 min), the reaction mixture was rapidly heated to 200 °C (~2 min) and held there for 30 min. After cooling to room temperature, the product w-CoO particles were precipitated with ethanol, centrifuged, washed several times with methanol and acetone, and resuspended in toluene. Following isolation and purification, all particles were easily dispersed in toluene to give colloidal suspensions of high optical quality, as shown in Figure 1a. Quantitative cobalt and zinc concentrations were determined by inductively coupled plasma atomic emission spectroscopy (ICP-AES, Jarrel Ash model 955).

Scanning electron microscopy (SEM) images were collected with a FEI Sirion scanning electron microscope at a 10 kV accelerating voltage using through-lens detection on one drop of dilute colloidal suspension deposited on a silicon wafer. Transmission electron microscopy (TEM) images and electron diffraction images were collected with a JEOL 2010 transmission electron microscope at the Pacific Northwest National Laboratories. Powder X-ray diffraction (XRD) data were collected by a Rigaku Rotaflex RTP300 X-ray diffractometer. Magnetic data were collected with a Quantum Design MPMS-5 SQUID magnetometer on sealed air-free colloidal suspensions in toluene. The linear magnetization measured at room temperature was used to estimate the background to be subtracted from the low temperature data for analysis (see discussion).

Electronic absorption spectra were collected using a Cary 500 (Varian) spectrophotometer on free-standing colloids either as dilute toluene suspensions (room temperature) or as frozen oleylamine

(18) Alaria, J.; Cheval, N.; Rode, K.; Venkatesan, M.; Coey, J. M. D. *J. Phys. D: Appl. Phys.* **2008**, *41*, 135004.
(19) Kodama, R. H. *J. Magn. Magn. Mater.* **1999**, *200*, 359–372.
(20) Winkler, E.; Zysler, R. D.; Mansilla, M. V.; Fiorani, D. *Phys. Rev. B* **2005**, *72*, 132409.
(21) Richardson, J. T.; Yiagas, D. I.; Turk, B.; Forster, K.; Twigg, M. V. *J. Appl. Phys.* **1991**, *70*, 6977–6982.
(22) Radovanovic, P. V.; Norberg, N. S.; McNally, K. E.; Gamelin, D. R. *J. Am. Chem. Soc.* **2002**, *124*, 15192–15193.
(23) Schwartz, D. A.; Norberg, N. S.; Nguyen, Q. P.; Parker, J. M.; Gamelin, D. R. *J. Am. Chem. Soc.* **2003**, *125*, 13205–13218.
(24) Lommens, P.; Smet, P. F.; de Mello Donegá, C.; Meijerink, A.; Piraux, L.; Michotte, S.; Mátéfi-Tempfli, S.; Poelman, D.; Hens, Z. *J. Lumin.* **2006**, *118*, 245–250.
(25) Liu, W. K.; Whitaker, K. M.; Kittilstved, K. R.; Gamelin, D. R. *J. Am. Chem. Soc.* **2006**, *128*, 3910–3911.
(26) Clavel, G.; Willinger, M.-G.; Zitoun, D.; Pinna, N. *Adv. Funct. Mater.* **2007**, *17*, 3159–3169.
(27) Volbers, N.; Zhou, H.; Knies, C.; Pfisterer, D.; Sann, J.; Hofmann, D. M.; Meyer, B. K. *Appl. Phys. A: Mater. Sci. Process.* **2007**, *88*, 153–155.
(28) Lommens, P.; Lambert, K.; Loncke, F.; Muynck, D. D.; Balkan, T.; Vanhaecke, F.; Vrielinck, H.; Callens, F.; Hens, Z. *Chem. Phys. Chem.* **2008**, *9*, 484–491.
(29) Pereira, A. S.; Ankiewicz, A. O.; Gehlhoff, W.; Hoffmann, A.; Pereira, S.; Trindade, T.; Grundmann, M.; Carmo, M. C.; Sobolev, N. A. *J. Appl. Phys.* **2008**, *103*, 07D140.
(30) Redman, M. J.; Steward, E. G. *Nature* **1962**, *193*, 867.
(31) Han, M. J.; Yu, J. *J. Korean Phys. Soc.* **2006**, *48*, 1496–1500.
(32) Archer, T.; Hanafin, R.; Sanvito, S. *Phys. Rev. B* **2008**, *78*, 014431.
(33) Li, Y.; Afzaal, M.; O'Brien, P. *J. Mater. Chem.* **2006**, *16*, 2175–2180.

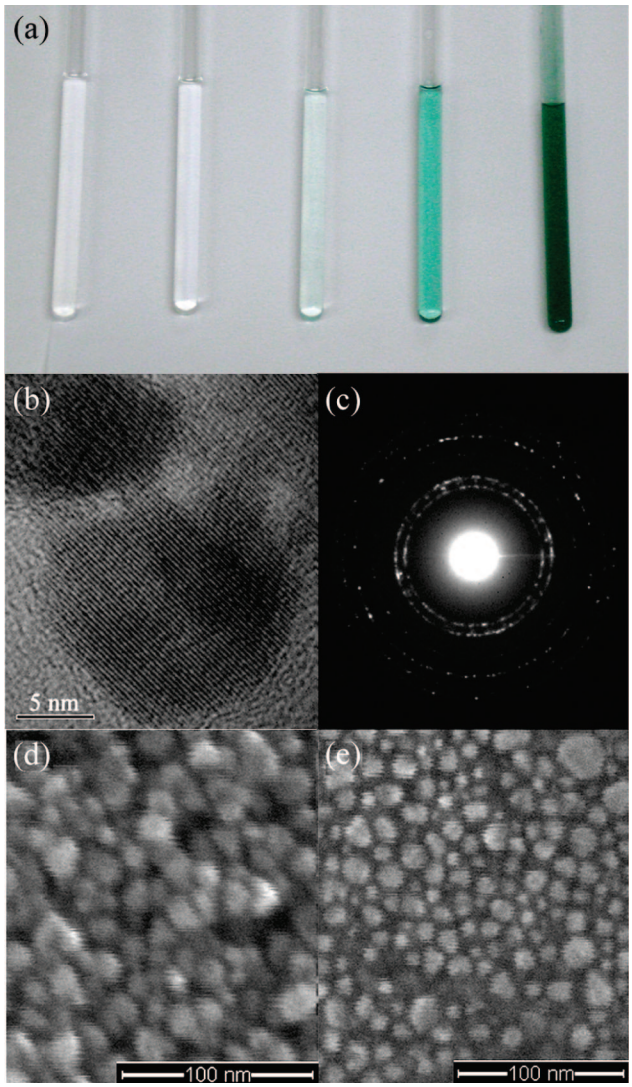

Figure 1. (a) Color photograph of dilute colloidal suspensions of $Zn_{1-x}Co_xO$ nanocrystals at various values of x, showing the high optical qualities of the suspensions and the deepening color as x is increased. From left to right, $x = 0.0$ (w-ZnO), 0.0075, 0.054, 0.319, and 1.0 (w-CoO). (b) TEM image of a w-CoO ($x = 1.0$) particle aproximately 20 nm in diameter with visible lattice fringes and crystal facets. (c) Electron diffraction pattern for the for CoO particles collected using an ~1 μm spot size, indicating wurtzite structure. SEM images of (d) w-CoO and (e) $Zn_{1-x}Co_xO$ ($x = 0.319$) nanocrystals.

glasses deposited on quartz substrates (20 K, He Displex closed-cycle refrigerator). MCD spectra were collected on the same frozen suspensions using an Aviv 40DS spectropolarimeter and a high-field superconducting magneto-optical cryostat (Cryo-Industries SMC-1659 OVT) with a variable-temperature sample compartment positioned in the Faraday configuration. MCD intensities were measured as the differential absorbance, $\Delta A = A_L - A_R$, where A_L and A_R refer to the absorption of left and right circularly polarized photons following the sign convention of Piepho and Schatz,[34] and they are reported as θ (mdeg) = 32980 ΔA.

III. Results and Analysis

A. General Materials Characterization. Figure 1 shows representative (a) photographic, (b) TEM, (c) electron diffraction, and (d, e) SEM images of the various nanocrystals investigated. With increasing x, the green colors of the colloidal suspensions deepen, reaching an attractive forest green at w-CoO (Figure 1a). The TEM and SEM images of the w-CoO nanocrystals (Figure 1b,d) show crystalline particles of various sizes between 5 and 30 nm diameter. Some evidence of hexagonal faceting is apparent. The selected area electron diffraction pattern shown in Figure 1c indicates a wurtzite lattice structure. Figure 2 shows the powder XRD patterns for a series of samples with increasing x (a−e) and the calculated peak positions for the main crystallographic phases of cobalt and zinc oxides (f−i). Comparison indicates that these crystals all have the wurtzite lattice structure. Notably, no peaks from CoO in the rock salt structure (Figure 2h), its thermodynamically stable form,[35] or in the zinc blende structure (Figure 2i) could be detected. The inset of Figure 2 shows the region between 36° and 43° on a logarithmic scale to emphasize the absence of the two intense fcc-CoO peaks expected at 36.5° and 42.4°. Although the fcc peak at 36.5° might be hidden under the wurtzite peak at 36.3°, the peak at 42.4° should be clearly observable if appreciable fcc-CoO was formed during synthesis. Other oxides such as Co_3O_4 were also not observed. There is a small shift of all peaks with increasing x, caused by a contraction of the unit cell volume from 47.66 ($x = 0.0$) to 47.64 Å^3 ($x = 1.0$), consistent with the slightly smaller tetrahedral ionic radius of cobalt (Zn^{2+}, 0.60 Å; Co^{2+}, 0.56 Å).[36]

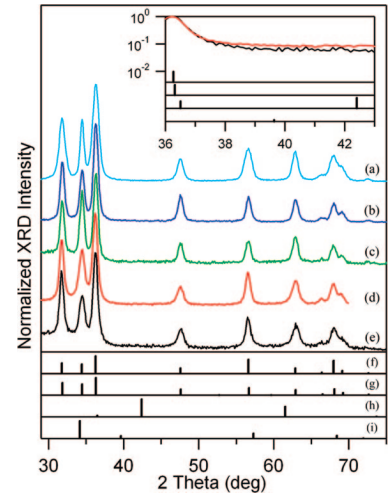

Figure 2. XRD of $Zn_{1-x}Co_xO$ nanocrystals. $x =$ (a) 0.0 (w-ZnO), (b) 0.0075, (c) 0.054, (d) 0.319, and (e) 1.0 (w-CoO), all normalized to the most intense peak and offset vertically for clarity. Calculated peak positions for (f) w-ZnO, (g) w-CoO, (h) fcc-CoO, and (i) zinc blende CoO. Inset: XRD intensities ($x = 1.0$ and 0.319) between 36° and 43° plotted on a logarithmic intensity scale.

From a Scherrer analysis[37] of the widths of the XRD peaks, the w-CoO particles have an estimated average diameter of $d \sim 30$ nm. The other samples also have diameters of $d \sim 30$ nm based on this analysis, in agreement with the sizes of the larger particles seen in Figure 1d. Because the quantum confinement regime of ZnO is much

(34) Piepho, S. B.; Schatz, P. N. *Group Theory in Spectroscopy with Applications to Magnetic Circular Dichroism*, Wiley, New York, U.S.A., 1983.

(35) Liu, J. F.; Yin, S.; Wu, H. P.; Zeng, Y. W.; Hu, X. R.; Wang, Y. W.; Lv, G. L.; Jiang, J. Z. *J. Phys. Chem. B* **2006**, *110*, 21588–21592.

(36) Lide, D. R. *CRC Handbook of Chemistry and Physics*; CRC Press/Taylor and Francis: Boca Raton, FL, 2007; p 1008.

(37) West, A. R. *Solid State Chemistry*; Wiley: Chichester, 1992.

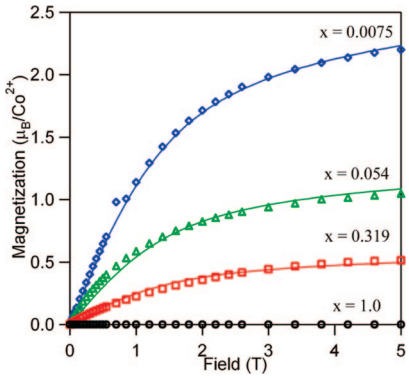

Figure 3. Magnetization per cobalt for colloidal samples of $Zn_{1-x}Co_xO$ for $x = 0.0075$ (blue, ◇), 0.054 (green, △), 0.319 (red, □), and 1.0 (black, ○). The values for x_{eff}/x are 0.74, 0.36, 0.165, and 6.5×10^{-5}, respectively.

smaller, beginning at $d \sim 7$ nm, there should be no size effects on the electronic properties of this series of particles. Furthermore, all of these nanocrystals are comparable in size to the NiO nanocrystals that do show hystereses due to uncompensated surface spins.[20,21] They are also similar in size to the spinodal decomposition nanostructures found in $Zn_{1-x}Cr_xTe$ ($d \sim 50$ nm),[7] but they are somewhat larger than the spinodal nanostructures found in $Ga_{1-x}Mn_xAs$ ($d \sim 3$ nm).[38] The magnetic measurements effectively probe all sizes within these large size dispersions. Moreover, for $x = 0.319$, the enormous variety of microscopic spatial arrangements of dopants within the ensemble of nanocrystals covers a very broad range of possible spinodal domain configurations within the wurtzite ZnO lattice structure, including those described in proposals of spinodal ferromagnetism in $Zn_{1-x}Co_xO$.[5,11−13,39]

B. Magnetization. To evaluate the possibility that dopant enrichment via spinodal decomposition might be responsible for the ferromagnetic-like magnetism of $Zn_{1-x}Co_xO$, magnetization measurements were performed on this series of nanocrystals at several temperatures between 2 and 300 K. Figure 3 shows the 2 K field-dependence of the magnetization of the freestanding nanocrystals in colloidal suspension, after a correction to remove the linear response measured at 300 K. This linear response comes largely from the solvent diamagnetism but also contains the response of the antiferromagnetic lattice in the case of w-CoO, as described below. The average magnetic moment per Co^{2+} ion decreases with increasing x, as expected from nearest-neighbor antiferromagnetic superexchange interactions: at higher Co^{2+} concentrations, there is a larger fraction of antiferromagnetically coupled Co^{2+} ions present that makes negligible contributions to the magnetization. The nearest-neighbor superexchange interactions in diluted $Zn_{1-x}Co_xO$ have been found to be antiferromagnetic with an effective exchange integral (J) on the order of -20 cm^{-1} (using the $-2J$ Heisenberg exchange Hamiltonian),[40,41] leading to a total exchange splitting of approximately 240 cm^{-1} for a $Co^{2+}-Co^{2+}$ nearest-neighbor dimer, that is, much bigger than the thermal energy at 2 K. Density functional calculations have suggested ferromagnetic pairwise nearest-neighbor $Co^{2+}-Co^{2+}$ interactions along the axial direction in $Zn_{1-x}Co_xO$ and stronger antiferromagnetic exchange coupling for all other nearest neighbor $Co^{2+}-Co^{2+}$ interactions.[42]

$$\mathscr{H} = D\left(\hat{S}_Z^{\,2} - \frac{1}{3}S(S+1)\right) + g\mu_B \mathbf{SH} \qquad (1)$$

The spin Hamiltonian, eq 1, was used to calculate the energy splitting of the Co^{2+} ground state. In eq 1, the ground-state spin is $S = 3/2$, the Landé factor is $g = 2.27$, and the axial zero-field splitting is $2D = 5.44$ cm^{-1}.[43,44] From the calculated energies the magnetization was derived as the numerical derivative of the energies versus magnetic field. Averaging over all possible orientations of the magnetic field with respect to the cation z-axis yielded M_{calc}, which was scaled according to eq 2 to fit the experimental orientation-averaged magnetization curves, shown as solid lines in Figure 3. The $Zn_{1-x}Co_xO$ samples with small x can be expected to be described well by eq 1 because their magnetism is dominated by the isolated paramagnetic Co^{2+} ions. With increasing x the number of Co^{2+} ions without a nearest-neighbor Co^{2+} ion decreases and the contribution of larger clusters with uncompensated spins (e.g., $(Co^{2+})_3$) should become more important. At $x = 1.0$ all of the spins of internal Co^{2+} ions are antiferromagnetically paired, and the magnetization is consequently very small. After subtraction of a linear term (vide infra), a saturating magnetization curve is obtained that is similar to those measured at smaller x but ~10 000 times smaller (Supporting Information).

$$M = (x_{eff}/x)M_{calc} \qquad (2)$$

To fit the experimental data for the $Zn_{1-x}Co_xO$ series, the calculated magnetization was scaled by the effective concentration (x_{eff}/x) as described by eq 2, yielding the curves shown in Figure 3. For the colloidal $Zn_{1-x}Co_xO$ samples, under all measurement conditions, there was no evidence of any collective magnetization resembling the widely reported ferromagnetism of $Zn_{1-x}Co_xO$ materials. The fact that both the $x = 0.319$ and 1.0 samples show similar paramagnetic magnetization curves at 2 K indicates that the uncompensated surface spins are weakly coupled to the paired spins (i.e., small exchange bias). The magnetism at $x = 1.0$ and $x \ll 1.0$ both agree well with previous results,[15,16,44] and the magnetism at $x = 0.319$ shows that no cooperative magnetization or hysteresis is observed in highly dopant-enriched $Zn_{1-x}Co_xO$ nanocrystals either. The latter is the composition regime most closely related to the proposed spinodal decomposition phase, which is generally referred to as magnetic-ion rich rather than magnetic-ion pure (e.g., "Co-rich w-(Zn,Co)O nanocrystals" in ref 11). It is therefore concluded that cobalt enrichment in nanoscale volumes due

(38) Yokoyama, M.; Yamaguchi, H.; Ogawa, T.; Tanaka, M. *J. Appl. Phys.* **2005**, *97*, 10D317.
(39) Sato, K.; Katayama-Yoshida, H.; Dederichs, P. H. *Jpn. J. Appl. Phys.* **2005**, *44*, L948–L951.
(40) Sati, P.; Deparis, C.; Morhain, C.; Schäfer, S.; Stepanov, A. *Phys. Rev. Lett.* **2007**, *98*, 137204.
(41) Kim, J. H.; Kim, H.; Kim, D.; Yoon, S. G.; Choo, W. K. *Solid State Comm.* **2004**, *131*, 677–680.
(42) Pemmaraju, C. D.; Hanafin, R.; Archer, T.; Braun, H. B.; Sanvito, S. *Phys. Rev. B* **2008**, *78*, 054428
(43) Koidl, P. *Phys. Rev. B* **1977**, *15*, 2493–2499.
(44) Brumage, W. H.; Dorman, C. F.; Quade, C. R. *Phys. Rev. B* **2001**, *63*, 104411.

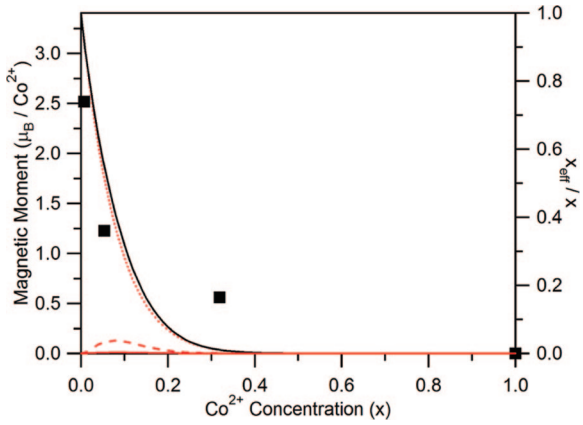

Figure 4. Magnetic moment per cobalt for colloidal samples of $Zn_{1-x}Co_xO$ for $x = 0.0075$, 0.054, $x = 0.319$, and $x = 1.0$. The curves denote the calculated probabilities of finding isolated dopant ions (dotted line), open trimers (dashed line), closed trimers (dashed and dotted line), and the total calculated moment from these clusters (solid line). Error in the experimental concentration determination (~3% of measured value) yields error bars smaller than the sizes of the symbol.

to spinodal decomposition cannot be solely responsible for the appearance of ferromagnetism in the magnetic semiconductor $Zn_{1-x}Co_xO$.

Also from Figure 4, the magnetic moment per Co^{2+} drops somewhat more rapidly with x than anticipated from a random statistical distribution of substitutional Co^{2+} ions within the lattice. In the low-doping regime ($x \leq 0.05$) the magnetization should be dominated by contributions from single ions and trimers (open and closed), while dimers have a negligible contribution to the magnetism and larger clusters only become important for higher concentrations. In Figure 4, the experimental average magnetic moment ($\mu = (x_{eff}/x)gS$) is plotted as a function of x, together with the expected moment for a statistical dopant distribution.[45] The experimental magnetic moments shown in Figure 4 have been derived from the scaling factors x_{eff}/x that were determined in Figure 3. The dashed curves in Figure 4 represent the contributions from $n = 1$ and $n = 3$ $(Co^{2+})_n$ clusters, based on their calculated statistical abundance and their corresponding magnetic moment. This comparison is only expected to be reasonable in the low-doping regime, because above approximately $x = 0.05$ the contributions of larger clusters become important but are very complicated to account for quantitatively. Nevertheless, it is clearly seen that even at small x the experimental average magnetic moment is significantly smaller than the one expected from statistical Co^{2+} doping (e.g., x_{eff}/x(expt.) = 0.74 and x_{eff}/x(stat.) = 0.92 for $x = 0.0075$). These data thus show that superstatistical Co^{2+} clustering within ZnO does not on its own lead to superparamagnetism or ferromagnetism.

C. Evolution of Electronic Structure from $Zn_{1-x}Co_xO$ to w-CoO. We now turn to experimental description of the electronic structure of $Zn_{1-x}Co_xO$ as it evolves from the DMS limit ($x \ll 1.0$) to w-CoO with increasing x. As mentioned above, the simple binary oxide w-CoO has not been studied extensively because it is a metastable phase. Recently, there have been several reports of w-CoO preparation and structural properties,[15−18,33,35,46,47] a few studies of its magnetism,[15−18] a study of its XAS (complicated by an impurity phase),[17] and a few studies of its electronic structure using first-principles electronic structure calculations.[15,31,32] There is remarkable little experimental electronic structural information available, and to the best of our knowledge even the optical absorption spectrum of w-CoO has not previously been reported. To understand the electronic structural evolution along this series of materials, the low-energy excited states of these materials were investigated.

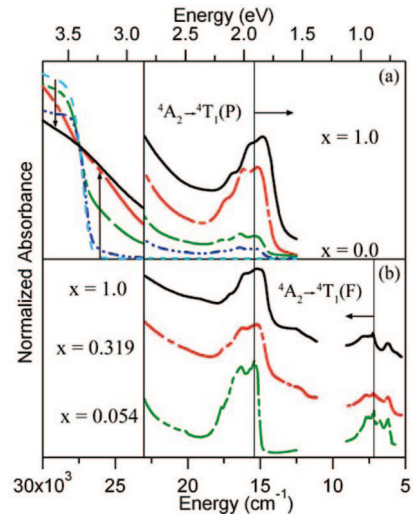

Figure 5. (a) Room-temperature and (b) low-temperature (20 K) electronic absorption spectra of $Zn_{1-x}Co_xO$ with $x = 0.0$, 0.0075, 0.054, 0.319, and 1.0. Arrows indicate changes with increasing x. The room-temperature spectra have been normalized at 27 500 cm^{-1}. The low temperature spectra have been normalized at the maxima of their $^4T_1(P)$ features and are offset vertically for clarity. The molar absorptivity of the $^4T_1(P)$ band in w-CoO is $\varepsilon_{Co^{2+}}(max) \approx 470$ M^{-1} cm^{-1}.

Figure 5 shows the normalized room- and low-temperature electronic absorption spectra of a series of $Zn_{1-x}Co_xO$ nanocrystals with $0.0 \leq x \leq 1.0$, and Figure 6 shows 5 K MCD spectra collected for $x = 0.0075$ and 1.0 nanocrystals as a function of magnetic field (0 to 5 T). The excited states observed in the absorption and MCD spectra of paramagnetic $Zn_{1-x}Co_xO$ in the dilute limit have been described in detail previously.[23,43,48] In general, three types of transitions are observed below ~30 000 cm^{-1} (3.72 eV):

(i) At low energies (16 700, 7000, and 4000 cm^{-1}), relatively weak and structured absorption bands are observed that are associated with the Co^{2+} $^4A_2 \rightarrow {}^4T_1(P)$, $^4T_1(F)$, and $^4T_2(F)$ d−d transitions.[43,48] The lowest-energy d−d transition ($^4A_2 \rightarrow {}^4T_2(F)$) occurs at 4000 cm^{-1} in dilute Co^{2+}-doped ZnO[43] and could not be detected in our samples because of occlusion by solvent and ligand absorption at these low energies. The $^4T_1(F)$ band was observed in the frozen matrix samples (Figure 5b), but it could not be observed in the toluene suspensions (Figure 5a) because of strong solvent absorption in the same energy region. The energies, band shapes, and relative intensities of both of the d−d features observed in the $x \ll 1.0$ samples agree well with those

(45) Shapira, Y.; Foner, S.; Ridgley, D. H.; Dwight, K.; Wold, A. *Phys. Rev. B.* **1984**, *30*, 4021–4023.
(46) Liu, J. F.; He, Y.; Chen, W.; Zhang, G. Q.; Zeng, Y. W.; Kikegawa, T.; Jiang, J. Z. *J. Phys. Chem. C* **2007**, *111*, 2–5.
(47) Meyer, W.; Hock, D.; Biedermann, K.; Gubo, M.; Müller, S.; Hammer, L.; Heinz, K. *Phys. Rev. Lett.* **2008**, *101*, 016103.
(48) Weakliem, H. A. *J. Chem. Phys.* **1962**, *36*, 2117–2140.

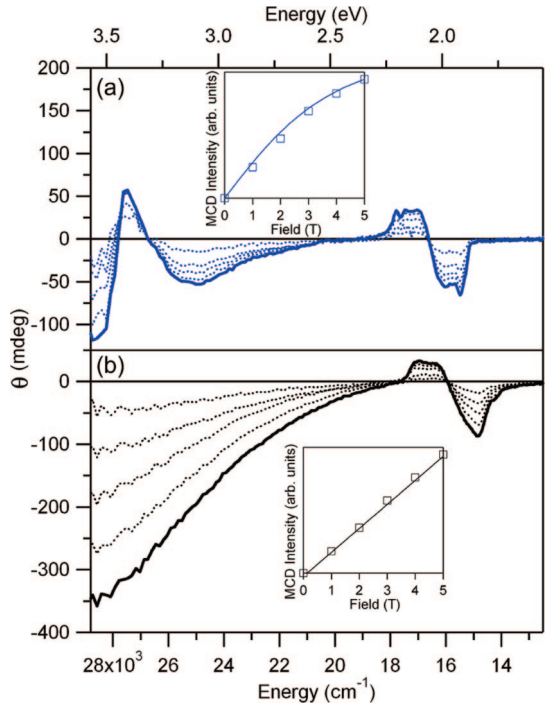

Figure 6. MCD spectra of (a) $x = 0.0075$ and (b) $x = 1.0$ collected at 5 K between 0 and 5 T. The insets show the optically detected MCD saturation magnetization curves for the two samples. The solid line in the inset of (a) is the calculated magnetization curve (see text) for paramagnetic Co^{2+} in ZnO, and the solid line in the inset of (b) is the best fit straight line.

observed in bulk single crystal samples with $x \leq 0.01$.[43,48] These transitions are described well by ligand-field theory, a model that treats d orbitals as highly localized at the cation. From Figure 6, the $^4A_2 \rightarrow {}^4T_1(P)$ transition at 16 700 cm^{-1} gives rise to a derivative-shaped *C*-term MCD intensity. The shape of this band in both absorption and MCD is largely determined by pseudo-first-order spin−orbit coupling within the $^4T_1$ manifold, but it is complicated enormously by configuration interaction between the resulting spinors and those derived from the numerous nearby states of doublet parentage. Still, this transition appears as a derivative-shaped MCD feature with near adherence to the intensity sum rule, as would be the case if the primary intensity gaining mechanism were first-order spin−orbit coupling within the $^4T_1(P)$ manifold.[34]

(ii) At the high-energy side of the spectrum, an *A*-term MCD feature is observed in Figure 6b that coincides with the ZnO band edge absorption in Figure 5a and that gains its MCD intensity through sp−d exchange, as discussed previously.[23,49,50]

(iii) Just below the ZnO band-edge transition, a broad sub-bandgap absorption and MCD feature is observed at ∼26 000 cm^{-1} that is assigned as an acceptor-type charge transfer (CT) transition involving promotion of a valence band (oxo 2p) electron to the Co^{2+} dopant (i.e., $Co^{2+} \rightarrow Co^{+} + h_{VB}{}^{+}$, or $L_{VB}MCT$).[23,51,52] The onset of this transition is not well

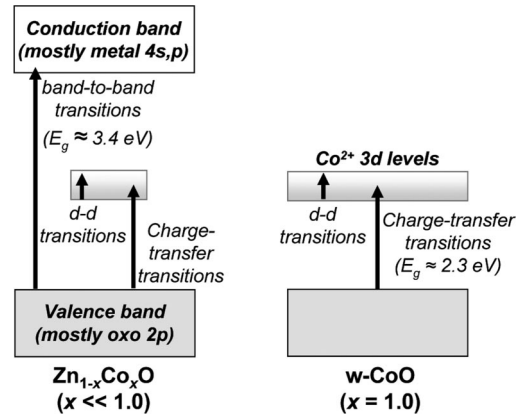

Figure 7. Schematic illustration of the optical transitions observed in (a) $Zn_{1-x}Co_xO$ ($x \ll 1.0$) and their evolution to the transitions observed in (b) w-CoO.

defined, and its tailing intensity can be observed down to ∼20 000 cm^{-1} (∼2.5 eV). On its high-energy side, this broad CT feature overlaps with the band-edge absorption and MCD of the ZnO host lattice, which distorts its shape. The small energy difference between the CT and band-to-band excitations in $Zn_{1-x}Co_xO$ has been related to the $Co^{2+}-e^{-}$ carrier binding energies and indicates that Co^{2+} has an appropriate potential to be in resonance with a shallow donor defect band.[52]

These three types of transitions are summarized in Figure 7a. A fourth transition ($Co^{2+} \rightarrow Co^{3+} + e_{CB}{}^{-}$, or $ML_{CB}CT$) has also been observed by photocurrent action spectroscopy,[51,52] but this transition carries very little oscillator strength and it is not clearly observed by absorption or MCD spectroscopies. Importantly, all of the above MCD intensities in dilute $Zn_{1-x}Co_xO$ follow the $S = 3/2$ saturation magnetization of the $x = 0.0075$ sample, indicating that they all arise from isolated paramagnetic Co^{2+} dopants.

In addition to the spectra for small *x*, the data in Figures 5 and 6 show the evolution of these various spectral features as *x* is increased from the dilute limit of $Zn_{1-x}Co_xO$ up to $x = 1.0$ (w-CoO). With increasing *x*, the $^4A_2 \rightarrow {}^4T_1(F)$ transition broadens only slightly and the central feature in the fine structure (6775 cm^{-1}) becomes less prominent. This band shows a blue shift with increasing *x*. Taking its sharp maximum as ∼7200 cm^{-1} as the reference point, the shift amounts to $\Delta E = +47$ cm^{-1} between $x = 0.054$ and 1.0, measured at 20 K, or ∼+0.5 cm^{-1}/% Co^{2+} on average. The $^4A_2 \rightarrow {}^4T_1(P)$ transition centered at ∼16 000 cm^{-1} broadens slightly more than the $^4T_1(F)$ with increasing *x*, and it shifts in the opposite direction, that is, toward lower energy. Using the lowest-energy local maximum of this band as the reference (∼15 400 cm^{-1}), this band shifts approximately −300 cm^{-1} at 20 K and −600 cm^{-1} at 300 K upon increasing *x* from 0.054 to 1.0 (i.e., ∼−3.2 cm^{-1}/% Co^{2+} at 20 K, and −6.3 cm^{-1}/% Co^{2+} at room temperature on average). The greater red shift of this band with *x* observed at room temperature than at cryogenic temperature is suggestive of thermal population of magnetic spin ladders in $(Co^{2+})_n$ clusters, as described previously for several other

(49) Ando, K.; Saito, H.; Jin, Z.; Fukumura, T.; Kawasaki, M.; Matsumoto, Y.; Koinuma, H. *J. Appl. Phys.* **2001**, *89*, 7284–7286.
(50) Pacuski, W.; Ferrand, D.; Cibert, J.; Deparis, C.; Gaj, J. A.; Kossacki, P.; Morhain, C. *Phys. Rev. B* **2006**, *73*, 035214.
(51) Liu, W.; Salley, G. M.; Gamelin, D. R. *J. Phys. Chem. B* **2005**, *109*, 14486–14495.
(52) Kittilstved, K. R.; Liu, W. K.; Gamelin, D. R. *Nat. Mater.* **2006**, *5*, 291–297.

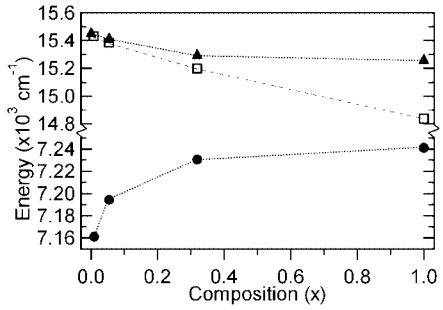

Figure 8. Plot of Co^{2+} d−d transition energies vs composition, *x*. Solid symbols represent low temperature (20 K) data and open symbols represent room temperature (298 K) data. The $^4A_2 \rightarrow {}^4T_1(P)$ transition shifts to lower energy with increasing *x* (squares and triangles), whereas the $^4A_2 \rightarrow {}^4T_1(F)$ transition shifts to higher energy (circles). Low temperature points for the lowest concentration sample are bulk single crystal measurements from ref 43 ($^4T_1(F)$) and ref 48 ($^4T_1(P)$). The dashed lines are guides for the eye.

lattices[53,54] and molecular clusters[55,56] containing magnetic ions. The shifts in the d−d transitions with *x* are summarized in Figure 8.

To explain the shifts of the d−d absorption bands with *x*, the changes in ligand-field parameters as a function of *x* were analyzed. Within the ligand-field theory model, the energies of the d−d excited states of tetrahedral Co^{2+} are predominantly determined by the parameters *Dq*, *B*, and *C* (generally fixed with respect to *B*), as described by the Tanabe-Sugano matrices.[57] From these matrices, the expressions in eq 3 give the energies of the two $^4T_1$ d−d transitions observed in Figure 5.

$$^4A_2 \rightarrow {}^4T_1(F): \quad E/B = \frac{1}{2}\{15 + 3(10Dq/B) - \sqrt{(225 - 18(10Dq/B) + (10Dq/B)^2)}\} \quad (3a)$$

$$^4A_2 \rightarrow {}^4T_1(P): \quad E/B = \frac{1}{2}\{15 + 3(10Dq/B) + \sqrt{(225 - 18(10Dq/B) + (10Dq/B)^2)}\} \quad (3b)$$

Dq is found theoretically and empirically to be approximately proportional to a^{-5}, where *a* is the metal−oxo bond length.[58] Using the average unit cell sizes, the average cation−anion bond lengths (*a*) can be estimated as a function of *x*, from which *Dq* for w-CoO can be estimated relative to literature values for *Dq* in dilute $Zn_{1-x}Co_xO$. The average Zn^{2+}-oxo bond length was found to be 1.978 Å.[59] Assuming that the oxygen atom occupies exactly the same position in the slightly smaller w-CoO unit cell, an average Co^{2+}-oxo bond length of 1.975 Å can be estimated. The value of *Dq* = 400 cm^{-1} for Co^{2+} in ZnO[43] and the ratio of average cation−anion bond lengths for the two end points (a_{wZnO}/a_{wCoO} =1.0015) thus yields a predicted value of *Dq* = 403 cm^{-1} in w-CoO.

The shorter Co^{2+}−oxo bond length also induces greater metal−oxo covalency and thus decreases electron−electron repulsion via the nephelauxetic effect, as parametrized by the Racah parameters. From eq 2, a reduction of *B* from 760 cm^{-1} for dilute $Zn_{1-x}Co_xO$ (ref 43) to 736 cm^{-1} for w-CoO, while increasing *Dq* from 400 to 403.5 cm^{-1}, reproduces both the signs and the magnitudes of the experimental shifts very well: $\Delta E(^4A_2 \rightarrow {}^4T_1(P)) = -300$ cm^{-1}, $\Delta E(^4A_2 \rightarrow {}^4T_1(F)) = +47$ cm^{-1}). Comparable changes in *Dq* and *B* have been seen in Co^{2+}-doped CdTe crystals under hydrostatic pressure,[60] in $Cd_{1-x}Co_xGa_2S_4$ with increasing *x*,[61] and in Co^{2+}-doped $Cd_{1-x}Zn_xSe$ with increasing *x*.[62] Although the absolute values of *Dq* and *B* obtained here for w-CoO are subject to the same uncertainties as those determined for $Zn_{1-x}Co_xO$ (ref 43), the trends are reliable. This analysis thus demonstrates that the d−d absorption spectra of w-CoO can be described using ligand-field theory with reasonable parameters that are merely perturbed in the expected ways relative to those of dilute $Zn_{1-x}Co_xO$ due to a small Co^{2+}−oxo bond contraction with increasing *x*.

The small broadening of the d−d transitions at large *x* is attributed to inhomogeneous Co^{2+} environments. For example, within the internal volumes of the lattices, strain distribution occurs over multiple bond lengths[63,64] and will lead to broadening at intermediate values of *x*. Magnetic exchange interactions between neighboring Co^{2+} ions will lead to level splittings and therefore also spectral broadening as *x* increases.[53−56] Finally, during the recapping of the $Zn_{1-x}Co_xO$ nanocrystals at low *x*, surface bound Co^{2+} is removed and only internal Co^{2+} ions remain,[23] but in w-CoO there are always surface Co^{2+} ions, which have a slightly different coordination environment than the internal Co^{2+} ions and therefore also broaden the d−d absorption bands.

From the data in Figure 5a, increasing *x* leads to a decrease in the intensity of the ZnO band-edge absorption (∼28 500 cm^{-1}), while the CT intensity at ∼26 000 cm^{-1} increases. As seen in Figure 6, increasing *x* from ∼0.0 to 1.0 also eliminates the ZnO band-edge MCD intensity, but the d−d and CT MCD intensities remain. The increasing intensity of the CT transition with increasing Co^{2+} content is consistent with the description of this transition as an oxo → Co^{2+} CT excitation in the dilute limit.[23,51,52] This absorption feature in w-CoO has intensity tailing down to ∼19 000 cm^{-1} (2.36 eV) in Figure 6. Similar tails are observed in indirect band gap semiconductors like silicon,[65] suggesting that the band gap in w-CoO is also indirect. Such tails are frequently observed in transition-metal oxides, but

(53) Ferguson, J.; Guggenheim, H. J.; Tanabe, Y. *J. Phys. Soc. Jpn.* **1966**, *21*, 692–704.
(54) McClure, D. S. *J. Chem. Phys.* **1963**, *39*, 2850–2855.
(55) Decurtins, S.; Güdel, H.-U. *Inorg. Chem.* **1982**, *21*, 3598–3606.
(56) Schenker, R.; Weihe, H.; Güdel, H.-U.; Kersting, B. *Inorg. Chem.* **2001**, *40*, 3355–3362.
(57) Tanabe, Y.; Sugano, S. *J. Phys. Soc. Jpn.* **1954**, *9*, 753–766.
(58) Figgis, B. N.; Hitchman, M. A. *Ligand Field Theory and its Applications*; Wiley: New York, 2000.
(59) Albertsson, J.; Abrahams, S. C.; Kvick, A. *Acta Crystallogr.* **1989**, *B45*, 34–40.
(60) Gardavský, J.; Werner, A.; Hochheimer, H. D. *Phys. Rev. B* **1981**, *24*, 4972–4976.
(61) Kim, Y.-S.; Park, H.; Hyun, S.-C.; Jin, M.-S.; Park, G.-C.; Kim, C.-D.; Jang, K.; Choi, I.-H.; Kim, W.-T. *Phys. Status Solidi A* **2006**, *203*, 2924–2928.
(62) Santangelo, S. A.; Hinds, E. A.; Vlaskin, V. A.; Archer, P. I.; Gamelin, D. R. *J. Am. Chem. Soc.* **2007**, *129*, 3973–3978.
(63) Srivastava, G. P.; Martins, J. L.; Zunger, A. *Phys. Rev. B* **1985**, *31*, 2561–2564.
(64) Robouch, B. V.; Kisiel, A.; Konior, J. *J. Alloys. Compd.* **2002**, *339*, 1–17.
(65) Kittel, C. *Introduction to Solid State Physics*, 7th ed.; Wiley: New York, 1996.

they are not well understood.[66] Overall, the data suggest that w-CoO is formally a charge-transfer insulator with a 5 K indirect optical energy gap of $E_g \sim 2.3$ eV.

Notably, the w-CoO MCD intensities in Figure 6b depend linearly on applied magnetic field, confirming that they arise from the antiferromagnetic lattice. The linear dependence with increasing field in Figure 6b (inset) mirrors that of the magnetic data collected in Figure 3 for the same composition (Supporting Information), but this linear contribution has been subtracted out from the magnetization data because it cannot be reliably distinguished from the linear diamagnetic response of the solvent in these colloidal samples. The linear "diamagnetic" correction thus eliminates both the diamagnetic response and the linear response from the antiferromagnetic w-CoO. Similar linear corrections are routinely applied to eliminate substrate diamagnetism in epitaxial films, and any w-CoO signal present would therefore also be lost. From this comparison, it is evident that MCD spectroscopy is a superior probe for detection of antiferromagnetic spinodal domains in magnetic semiconductors compared to magnetic susceptibility.

The data in Figures 5, 6, and 8 allow several important conclusions to be drawn about the previously unexplored electronic structure of w-CoO. First, the observation of only a small shift in the d−d transition energies, without any significant change in band shape (Figure 6), suggests that the Co^{2+} d orbitals in w-CoO remain highly localized. The fact that the electronic transitions of w-CoO can be described very well by a local model like ligand-field theory suggests that there is no major dispersion of the d bands in this material. This conclusion contrasts with the electronic structure description of w-CoO derived from spin-polarized LMTO or LSDA calculations, which suggest large dispersion of the d bands and consequently a metallic ground state.[15] As already emphasized by these and other authors,[15,31,32] such calculations underestimate the band gap energy and describe the nature of the gap poorly because they neglect on-site Coulomb interactions (U_d), which are large for Co^{2+}. It also follows from the observation of the $^4A_2 \rightarrow {}^4T_1(P)$ and $^4A_2 \rightarrow {}^4T_1(F)$ d−d transitions in w-CoO that the Co^{2+} ions retain their $^4A_2$ ground states, that is, that they are high-spin $S = 3/2$ in their local configuration. The very similar d−d transition energies (and ligand-field parameters, Dq and B) of $Zn_{1-x}Co_xO$ and w-CoO further indicate that the Co^{2+}-oxo covalencies are also very similar in these two lattices.

Second, the data clearly show the evolution of the broad sub-bandgap feature of $Zn_{1-x}Co_xO$ at $\sim$26 000 cm^{-1} from an impurity-centered CT transition in the dilute limit into the band gap absorption of the new material, w-CoO, as x approaches 1.0. This observation strongly suggests that the band gap of w-CoO is largely of charge-transfer character, with an indirect energy gap of $\sim$2.3 eV at 5 K. This experimental optical energy gap is similar to but somewhat larger than the gap calculated from LSDA+U level of theory (1.50 eV, ref 31), which has also suggested an indirect energy gap. The relationship between the sub-bandgap CT transition in $Zn_{1-x}Co_xO$ and the optical energy gap in w-CoO is illustrated in Figure 7.

Interestingly, w-CoO could have been expected to be in the intermediate regime between Mott-Hubbard and charge-transfer insulator descriptions,[11] where the combined d−d Coulomb and exchange interaction (U_d) is on the same order of magnitude as the oxo $\rightarrow Co^{2+}$ charge-transfer energy (Δ).[67] In this case, the charge-transfer excitation of dilute $Zn_{1-x}Co_xO$ would incur some metal-to-metal charge-transfer character (i.e., $Co^{2+}Co^{2+} \rightarrow Co^{3+}Co^{1+}$) as x is increased. Typical experimental estimates of U_d for Co^{2+} in oxides are $\sim$5 eV.[68] Values of $U_d = 5.0$[32] and 6.0 eV[31] have been used for calculations of w-CoO, and $U_d = 5.0$ eV has been used for calculations of CoO in the cubic rock salt structure,[69] although values as small as 2.8 eV have also been used for calculations of Co^{2+} in dilute $Zn_{1-x}Co_xO$.[70] Analysis of the Co^{2+} 2p XPS spectrum using a configuration−interaction cluster model has yielded an experimental estimate of $U_d = 6.0 \pm 0.5$ eV, with other parameters of $\Delta = 5.0 \pm 0.5$ eV, $Dq = 565$ cm^{-1}, $B = 1115$ cm^{-1}, and $C = 4355$ cm^{-1}.[71] Note that the Racah parameters used for these cluster model calculations were fixed at what were quoted as free-ion values, but these values are found by the d−d spectroscopy to be reduced relative to the free ion due to Co^{2+}−oxo covalency (e.g., $B \approx 760$ cm^{-1}).[43,48] From the dilute $Zn_{1-x}Co_xO$ spectroscopy, the L_{VB}MCT energy Δ equals $\sim$3 eV (Figure 6a and refs 23, 51, and 52). Overall, the ratio of $U_d/\Delta \sim 1.0-2.0$ for w-CoO thus indicates that this material is likely best described as a charge-transfer insulator that approaches the intermediate regime within the Zaanen−Sawatzky−Allen (ZSA) phase diagram.[67] Additional experiments will be required to refine this description, but the experimental data in Figures 5 and 6 provide strong evidence suggesting that the band gap in w-CoO cannot be of predominantly Mott-Hubbard type.

IV. Conclusions and Discussion

A. Changes with *x*. A series of freestanding $Zn_{1-x}Co_xO$ nanocrystal samples has been synthesized, with $0.0 \leq x \leq 1.0$. Several well-behaved physical changes have been identified that correlate with changes in the composition parameter x:

(i) Increasing x decreases the size of the unit cell.

(ii) Increasing x leads to inhomogeneous broadening of the Co^{2+} d−d absorption bands at intermediate x.

(iii) Increasing x increases Dq and decreases B in ways that are consistent with the changing structural parameters as described by ligand-field theory. These changes are

(66) Allen, J. W. In *Magnetic Oxides*; Craik, D. J., Ed.; John Wiley & Sons: London, 1975; Vol. 1, p 349.

(67) Zaanen, J.; Sawatsky, G. A.; Allen, J. W. *Phys. Rev. Lett.* **1985**, *55*, 418–421.

(68) van Elp, J.; Wieland, J. L.; Eskes, H.; Kuiper, P.; Sawatzky, G. A.; de Groot, F. M. F.; Turner, T. S. *Phys. Rev. B* **1991**, *44*, 6090–6103.

(69) Pickett, W. E.; Erwin, S. C.; Ethridge, E. C. *Phys. Rev. B* **1998**, *58*, 1201–1209.

(70) Lany, S.; Raebiger, H.; Zunger, A. *Phys. Rev. B* **2008**, *77*, 241201(R).

(71) Kobayashi, M.; Ishida, Y.; Hwang, J. l.; Mizokawa, T.; Fujimori, A.; Mamiya, K.; Okamoto, J.; Takeda, Y.; Okane, T.; Saitoh, Y.; Muramatsu, Y.; Tanaka, A.; Saeki, H.; Tabata, H.; Kawai, T. *Phys. Rev. B* **2005**, *72*, 201201(R).

manifested in modest shifts of the d−d transition energies across the whole range of x.

(iv) Increasing x redistributes absorption and MCD intensity from the ZnO band-to-band feature to a Co^{2+}-centered L_{VB}MCT band, which eventually evolves into the CT-type band gap absorption of w-CoO. A 5 K-band gap energy of $\sim$19 000 cm^{-1} ($\sim$2.3 eV) is estimated for w-CoO.

(v) Increasing x decreases the magnetization per Co^{2+} due to antiferromagnetic coupling, with superstatistical Co^{2+} clustering at small x.

(vi) Increasing x adds a linear component to the field-dependence of the MCD intensity, which becomes the dominant field dependence at $x = 1.0$.

One or more of these changes should be useful for identification of spinodal decomposition in bulk or thin film $Zn_{1-x}Co_xO$. For these purposes, the shifted d−d transition energies and linear MCD response of the antiferromagnetic w-CoO appear to be most applicable, and it is concluded that MCD spectroscopy is a more sensitive probe of spinodal decomposition than magnetic susceptibility.

B. Relationship to Ferromagnetism in $Zn_{1-x}Co_xO$. None of the compositions studied here showed superparamagnetic or ferromagnetic responses under any of the conditions explored. This finding offers strong experimental evidence that spinodal decomposition alone cannot be the origin of the ferromagnetism in $Zn_{1-x}Co_xO$. This conclusion agrees well with recent experimental and theoretical investigations of the w-CoO phase, which show it to be an antiferromagnetically ordered lattice,[15−18] and it additionally rules out ferromagnetic signals from uncompensated surface spins in highly Co^{2+}-enriched $Zn_{1-x}Co_xO$ nanostructures. In view of these findings, it must be concluded that some other condition is ultimately necessary for ferromagnetism to be observed in dilute $Zn_{1-x}Co_xO$.

If not spinodal decomposition, then what? Current approaches to modeling this ferromagnetism struggle to describe the paradoxical combination of high ordering temperatures but small saturation moments and spinodal decomposition provided an attractive scenario for enhancing Co^{2+}−Co^{2+} exchange energies by bringing Co^{2+} ions closer together than in mean-field scenarios. Recent density functional calculations have suggested that high ordering temperatures might be achieved even with isotropic dopant distributions, given the right combination of specific dopant−defect pair concentrations and additional n-type charge carriers.[42] The role of the vacancy in these calculations is to bring the Co^{2+} d levels in resonance with shallow donor defects, but analysis of the CT transition observed in Figure 6 has shown that this condition is already met for substitutional Co^{2+} in ZnO.[52,72] In general, other DFT calculations concur about the importance of such dopant−donor energetic resonance.[70,73] Still, recent experiments on high-structural-quality Al:$Zn_{1-x}Co_xO$ films have demonstrated that just the combination of Co^{2+} and shallow donors is also not sufficient to induce ferromagnetism.[74]

Much like the phenomenological correlation between ferromagnetism and spinodal decomposition observed in $Zn_{1-x}Cr_xTe$,[7] there is a broad body of phenomenological evidence suggesting that ferromagnetism in $Zn_{1-x}Co_xO$ and several other related oxides is linked to the presence of extended structural defects.[23,72,75−88] In one series of studies, for example, aggregation of various paramagnetic doped oxide nanocrystals (including $Zn_{1-x}Co_xO$ such as those studied here) was found to induce partial ferromagnetic ordering, a phenomenon attributed to the formation of nonstoichiometric defects at the fusion interfaces.[23,76,77,79,84] The ferromagnetism of $Ti_{1-x}Cr_xO_{2-\delta}$ films grown by MBE was also found to track the grain boundary density very closely.[80,83] In another series of studies, exposure of $Zn_{1-x}Co_xO$ films to various reducing atmospheres was found to induce partial ferromagnetic ordering in a highly controlled and reversible manner.[72,81,82,85,89,90] AC impedance spectroscopy has shown a correlation between enhanced $Zn_{1-x}Co_xO$ ferromagnetic saturation moments and grain boundary defect densities induced by such low-temperature reductive annealing.[85] Faster donor diffusion into and out of polycrystalline ZnO films[72] than epitaxial ZnO films[82] was shown by monitoring the reversible appearance and disappearance of the characteristic near-IR shallow donor absorption band,[91] and the ferromagnetic saturation moments correlated *linearly* with this near-IR shallow donor absorption intensity over many cycles.[72,82] Recently, it was reported[92] that $Zn_{1-x}Co_xO$ films of extremely high structural quality behaved qualitatively differently from those studied previ-

(72) Schwartz, D. A.; Gamelin, D. R. *Adv. Mater.* **2004**, *16*, 2115–2119.
(73) Walsh, A.; Silva, J. L. F. D.; Wei, S.-H. *Phys. Rev. Lett.* **2008**, *100*, 256401.
(74) Kaspar, T. C.; Droubay, T.; Li, Y.; Heald, S. M.; Nachimuthu, P.; Wang, C. M.; Shutthanandan, V.; Johnson, C. A.; Gamelin, D. R.; Chambers, S. A. *New J. Phys.* **2008**, *10*, 055010.
(75) Archer, P. I.; Gamelin, D. R. *J. Appl. Phys.* **2006**, *99*, 08M107.
(76) Radovanovic, P. V.; Gamelin, D. R. *Phys. Rev. Lett.* **2003**, *91*, 157202.
(77) Bryan, J. D.; Heald, S. M.; Chambers, S. A.; Gamelin, D. R. *J. Am. Chem. Soc.* **2004**, *126*, 11640–11647.
(78) Hong, N. H.; Sakai, J.; Huong, N. T.; Poirot, N.; Ruyter, A. *Phys. Rev. B* **2005**, *72*, 045336.
(79) Archer, P. I.; Radovanovic, P. V.; Heald, S. M.; Gamelin, D. R. *J. Am. Chem. Soc.* **2005**, *127*, 14479–14487.
(80) Kaspar, T. C.; Heald, S. M.; Wang, C. M.; Bryan, J. D.; Droubay, T.; Shutthanandan, V.; Thevuthasan, S.; McCready, D. E.; Kellock, A. J.; Gamelin, D. R.; Chambers, S. A. *Phys. Rev. Lett.* **2005**, *95*, 217203.
(81) Khare, N.; Kappers, M. J.; Wei, M.; Blamire, M. G.; MacManus-Driscoll, J. L. *Adv. Mater.* **2006**, *18*, 1449–1452.
(82) Kittilstved, K. R.; Schwartz, D. A.; Tuan, A. C.; Heald, S. M.; Chambers, S. A.; Gamelin, D. R. *Phys. Rev. Lett.* **2006**, *97*, 037203.
(83) Kaspar, T. C.; Droubay, T.; Shutthanandan, V.; Heald, S. M.; Wang, C. M.; McCready, D. E.; Thevuthasan, S.; Bryan, J. D.; Gamelin, D. R.; Kellock, A. J.; Toney, M. F.; Hong, X.; Ahn, C. H.; Chambers, S. A. *Phys. Rev. B* **2006**, *73*, 155327.
(84) Wang, X.; Xu, J. B.; Ke, N.; Yu, J.; Wang, J.; Li, Q.; Ong, H. C.; Zhang, R. *Appl. Phys. Lett.* **2006**, *88*, 223108.
(85) Hsu, H. S.; Huang, J. C. A.; Chen, S. F.; Liu, C. P. *Appl. Phys. Lett.* **2007**, *90*, 102506.
(86) Liu, X. F.; Yu, R. H. *J. Appl. Phys.* **2007**, *102*, 083917.
(87) Song, C.; Pan, S. N.; Liu, X. J.; Li, X. W.; Zeng, F.; Yan, W. S.; He, B.; Pan, F. *J. Phys.: Condens. Matter* **2007**, *19*, 176229.
(88) Liu, X. J.; Song, C.; Zeng, F.; Pan, F. *J. Phys.: Condens. Matter* **2007**, *19*, 296208.
(89) Kittilstved, K. R.; Norberg, N. S.; Gamelin, D. R. *Phys. Rev. Lett.* **2005**, *94*, 147209.
(90) MacManus-Driscoll, J. L.; Khare, N.; Liu, Y.; Vickers, M. E. *Adv. Mater.* **2007**, *19*, 2925–2929.
(91) Halliburton, L. E.; Giles, N. C.; Garces, N. Y.; Luo, M.; Xu, C.; Bai, L.; Boatner, L. A. *Appl. Phys. Lett.* **2005**, *87*, 172108.
(92) Kaspar, T. C.; Droubay, T.; Heald, S. M.; Engelhard, M. H.; Nachimuthu, P.; Chambers, S. A. *Phys. Rev. B* **2008**, *77*, 201303(R)

ously: rather than reversibly inducing the intense shallow donor absorption and ferromagnetism, reducing atmosphere led only to irreversible film decomposition and a strong metallic EXAFS signal. The reduced granularity of these high structural quality films apparently limits shallow donor diffusion. All of these studies provide evidence that shallow donors at grain boundaries make important contributions to the high-T_C ferromagnetism of these materials.

In general, grain boundaries may possess much higher densities of donor defects than the ordered ZnO lattices, and they can even dominate the conductivities of highly granular materials.[93,94] In DMSs, the confinement potential provided by donors concentrated along extended grain boundaries would likely enhance dopant-carrier magnetic exchange interactions in this locale, thereby improving the thermal stability of magnetic polarons analogous to the confinement-induced stabilization of excitonic magnetic polarons already reported for other nanoscale DMSs.[95,96] Despite a rather large body of experimental evidence pointing in this direction, the roles of grain boundaries in oxide DMS ferromagnetism have not yet received much theoretical scrutiny. A literature search revealed only one ab initio investigation of grain boundaries in oxide DMSs,[97] but this study focused on the electronic structures of cobalt ions rather than on magnetic ordering effects as described here. The recent model of charge-transfer ferromagnetism in oxide nanoparticles[98] may be of particular significance when applied to such grain boundaries.

In summary, the experimental results presented here indicate that spinodal decomposition alone does not give rise to ferromagnetism or superparamagnetism in $Zn_{1-x}Co_xO$, and they encourage experimentalists and theoreticians to look elsewhere for explanations. Grain boundary effects are suggested to be the possibility that is most experimentally substantiated but least understood or theoretically explored. The localization of ferromagnetism along grain boundaries may explain the paradoxical combination of high ordering temperatures and low saturation moments observed in many oxide DMSs and may also provide an explanation for the puzzling disconnect between magnetic and magneto-transport properties of some $Zn_{1-x}Co_xO$ films.[11]

Acknowledgment. This work was funded by the NSF (CRC-0628252), the Dreyfus Foundation, and the Sloan Foundation. Postdoctoral fellowship support from the Swiss National Science Foundation (to S.T.O.) is gratefully acknowledged. TEM data were collected at the EMSL, a national scientific user facility sponsored by DOE's Office of Biological and Environmental Research, located at Pacific Northwest National Laboratory, operated for DOE by Battelle. The authors thank Dr. Chongmin Wang (PNNL) and Dr. Paul Archer (UW) for valuable assistance with the TEM measurements.

Supporting Information Available: Additional w-CoO magnetic data (two figures, PDF). This material is available free of charge via the Internet at http://pubs.acs.org.

CM802280G

(93) Lee, J.; Hwang, J.-H.; Mashek, J. J.; Mason, T. O.; Miller, A. E.; Siegel, R. W. *J. Mater. Res.* **1995**, *10*, 2295–2300.
(94) Jose, J.; Abdul Khadar, M. *Mater. Sci. Eng.* **2001**, *A304−306*, 810–813.
(95) Mackowski, S.; Gurung, T.; Nguyen, T. A.; Jackson, H. E.; Smith, L. M.; Karczewski, G.; Kossut, J. *Appl. Phys. Lett.* **2004**, *84*, 3337–3339.
(96) Bacher, G.; Schömig, H.; Scheibner, M.; Forchel, A.; Maksimov, A. A.; Chernenko, A. V.; Dorozhkin, P. S.; Kulakovskii, V. D.; Kennedy, T.; Reinecke, T. L. *Physica E* **2005**, *26*, 37–44.
(97) Gemming, S.; Janisch, R.; Schreiber, M.; Spaldin, N. A. *Phys. Rev. B* **2007**, *76*, 045204.
(98) Coey, J. M. D.; Wongsaprom, K.; Alaria, J.; Venkatesan, M. *J. Phys. D: Appl. Phys.* **2008**, *41*, 134012.